JZUS

Numerical model and multi-objective optimization analysis of vehicle vibration[*]

Peng GUO[1], Jun-hong ZHANG[‡2]

(*1State Key Laboratory of Engine, Tianjin University, Tianjin 300072, China*)
(*2Mechanical Engineering Department, Tianjin University Renai College, Tianjin 301636, China*)
E-mail: pengguo@tju.edu.cn; zhangjh@tju.edu.cn
Received Mar. 30, 2016; Revision accepted Sept. 26, 2016; Crosschecked Apr. 11, 2017

Abstract: It is crucial to conduct a study of vehicle ride comfort using a suitable physical model, and a precise and effective problem-solving method is necessary to describe possible engineering problems to obtain the best analysis of vehicle vibration based on the numerical model. This study establishes different types of vehicle models with different degrees of freedom (DOFs) that use different types of numerical methods. It is shown that results calculated using the Hamming and Runge-Kutta methods are nearly the same when the system has a small number of DOFs. However, when the number is larger, the Hamming method is more stable than other methods. The Hamming method is multi-step, with four orders of precision. The research results show that this method can solve the vehicle vibration problem. Orthogonal experiments and multi-objective optimization are introduced to analyze and optimize the vibration of the vehicle, and the effects of the parameters on the dynamic characteristics are investigated. The solution F_1 (vertical acceleration root mean square of the vehicle) reduces by 0.0352 m/s^2, which is an improvement of 7.22%, and the solution F_2 (dynamic load coefficient of the tire) reduces by 0.0225, which is an improvement of 6.82% after optimization. The study provides guidance for the analysis of vehicle ride comfort.

Key words: Vehicle model; Hamming method; Runge-Kutta method; Design of experiment; Multi-objective optimization
http://dx.doi.org/10.1631/jzus.A1600124   **CLC number:** TH133.31

1 Introduction

With the development of society, cars have become an indispensable part of people's lives. The demand for vehicle comfort is increasing, and vehicle ride comfort, in particular, has become the focus of research into vehicle dynamics. How to reduce the vibration from random excitation from the road or other vibration sources is a key problem for manufacturers and researchers. To achieve better ride quality, one of the most useful ways is to establish a numerical model to predict the vibration source, and

an effective method is then derived. However, an accurate model is usually difficult to establish and the precise method for solving the model is also difficult to determine. Despite this, several types of optimization methods have been introduced to improve the ride comfort of vehicles. Therefore, studying the numerical model of vehicle dynamics and its solution are very important.

As a vehicle travels on the road, excitations arising from irregularities on the road surface, forces of acceleration, the engine itself, and the inertial forces on a curved track cause discomfort to the driver and influence the vehicle's maneuverability. Multibody system is usually used to analyze the vehicle's handling, and the research can be conducted in terms of multi-rigid-body dynamics and flexible multibody dynamics. There are many analytical methods for

multi-rigid-body dynamics, such as the Newton-Euler method, Lagrange method, Kane method, and R-W method. Building a multi-degree of freedom (DOF) mathematical vehicle model using the Newton-Euler formulation and multibody dynamic simulation model has been refined to provide a good prediction when applied to numerical vehicle models for a controlled vibration simulation. With the development of computer-aided engineering and virtual reality techniques, virtual prototyping software, such as ADAMS, has been used extensively to predict vehicle behavior and is used by leading manufacturers to shorten product development lead-times and meet the challenges of today's complex design and optimization problems. Compared with multi-DOF dynamic simulation, the results calculated using sophisticated dynamic software packages generate more precise responses. However, the multi-DOF model can predict, with acceptable accuracy, an engineering result with a shorter computational time and minimum complexity.

Bae *et al*. (2000) proposed an efficient implementation algorithm for explicit numerical integration methods so that relatively low-cost computers could be used for a real-time simulation of multibody vehicle dynamics models. The Newton chord method has been used to solve the equations of motion and constraints. Hegazy *et al*. (1999) used ADAMS to establish a multi-DOF nonlinear multibody dynamic model of a vehicle, comprising the front and rear suspension, steering system, road wheels, tires, and vehicle inertia. Schmitke *et al*. (2008) used graph theory and symbolic computing to generate efficient models for multibody vehicle dynamics. In addition to the aforementioned analyses, many researchers have used other methods to validate the analysis conducted using multi-DOF analysis. Vaddi and Kumar (2014) proposed a nonlinear full-vehicle model with 14 DOFs for the simulation of vehicle ride and handling performance. Various handling characteristics obtained from this model were compared with those from a full-vehicle multibody dynamics model in ADAMS. A vehicle with 10 DOFs incorporating nonlinear damper and suspension kinematic profiles was mathematically modeled by Yuen *et al*. (2014). The model was then validated against a similar vehicle model in multibody dynamic software and other

conventional vehicle models by comparing the simulated results from the handling tests. A 14-DOF vehicle dynamic model was validated with a multibody simulation by Kadir *et al*. (2012). A nine-DOF vehicle dynamics model that considered several steering inputs was also validated by Nasir *et al*. (2012). The authors showed that the simulation results were fairly close to the multibody simulation.

There are many factors that affect the ride comfort of a vehicle, and the suspension system can be designed with the best combination of parameters to provide optimum vibration performance. In the multi-DOF vehicle system model, the variables for the model design and suspension system evaluation are the sprung mass, sprung stiffness, and damping, which determine the ride comfort and suspension deflection of the vehicle. These parameters indicate the limit of the motion of the vehicle body. To experience real ride comfort within the vehicle design, the more powerful the optimization approaches, the better the results that will be obtained. Thus, researchers have attempted to use various optimization methods to optimize the performance criteria of the vehicle suspension, such as the single-objective optimization algorithm, genetic algorithm (GA), and multi-objective GA. Among optimization studies on suspension design, many studies have been performed using single-objective optimization, which can be the summation of several performance criteria multiplied by the appropriate weighting factors (Baumal *et al*., 1998; Hegazy *et al*., 1999). Jamali *et al*. (2014) established a multi-objective optimization model to optimize a five-DOF vehicle model that was capable of predicting actual suspension performance with acceptable results. Tamboli and Joshi (1999) used a simple two-DOF half-car model without considering any practical constraints to simulate actual random road excitations. Their model employed nonlinear programming to optimize the suspension parameters. Mirzaei and Hassannejad (2007) applied GA optimization to a passive suspension system. This method was initially applied to a simple two-DOF half-car model and the results were also compared with those obtained using nonlinear programming. Gündoğdu (2007) used single-objective GA to optimize a four-DOF quarter-car model and suspension system to achieve the best ride comfort performance

of the vehicle. According to global criterion method (Rao, 1996), this single-objective was composed by four design objectives to form, such as head acceleration, crest factor, suspension deflection, and tire deflection.

In the literature reviewed, many researchers focused on the multi-DOF model and achieved the following: (1) the establishment of a vehicle model based on different DOFs; (2) vehicle vibration control based on a different algorithm; (3) optimization of the vehicle dynamics based on the multi-DOF model; (4) a comparison of the characteristics of the multi-DOF model and multibody simulation; (5) vibration control based on the multi-DOF model; (6) assessment of the effect of suspension and tires on vehicle ride comfort. Thite *et al*. (2011) used a four-DOF vehicle model to analyze the ride dynamic of heavy vehicles. Ikenaga *et al*. (2000) applied a seven-DOF vehicle model to evaluate the dynamic characteristics using an active suspension system. Sulaiman *et al*. (2012) presented a model for a seven-DOF full-vehicle that was validated to study the ride comfort of a heavy vehicle. Yuen *et al*. (2014) used a ten-DOF mathematical vehicle model that was coupled with a suspension kinematic profile to design the suspension. With the development of the model, some special problems were considered, such as the standing posture. Gupta (2007) established a 15-DOF linear damped lumped-parameter vehicle model with the standing posture. Nigam and Malik (1987) developed a 15-DOF linear undamped lumped-parameter model based on the anthropomorphic model, which also considered the standing posture. Reddy *et al*. (2015) used a 15-DOF human-seat vibratory model to couple a seven-DOF model to study the dynamic response of a human driver to vehicle vibrations.

In addition to the aforementioned analyses, there have been many researchers focused on vibration control and tire-suspension response analysis. Ekoru and Pedro (2013) presented a proportional-integral-derivative (PID)-based control method for active vehicle suspension systems based on a half-car model. To improve the efficiency and capacity use, He *et al*. (2015) conducted an investigation on an active-suspension linear quadratic Gaussian controller based on a seven-DOF full-vehicle mode. Soleymani *et al*. (2012) used a full-vehicle model

with eight DOFs to design front and rear suspensions using two separate fuzzy controllers. The road adhesion condition always changes at a relatively low frequency, and Campbell (1981) found suspensions and tires should possess many attributes for ride comfort, durability, and vehicle handling. von Chappuis *et al*. (2013) applied impulsive suspension loads to tire and suspension elements to study the reactions of jounce bumper-rebound stop and tire characteristics. Zong *et al*. (2011) considered the tire-road friction coefficient in the multi-DOF model to improve the precision of vehicle state estimation.

In the literature reviewed, most of the multi-DOF vehicle models were simplified. Some models ignored the effect of kinematic changes toward the tire or used a linear suspension kinematic model with a small angle assumption. A small number used a parametric model that coupled with kinematic profiles to simulate the effect of suspension kinematics.

To summarize, some types of multi-DOF models of a vehicle have been used to analyze the ride comfort of the vehicle, and the models are becoming increasingly complex. Most researchers have focused on the linear model; a small number of researchers have focused on the nonlinear model, and they have usually neglected the effect on solving methods from dynamic simulation and low-amplitude vibration ride comfort, such as from vibration transmitted from the road.

To gain an insight into vehicle dynamic characteristics, some types of vehicle dynamic simulation models have been established and are presented here, such as the quarter-vehicle model, half-vehicle model, and full-vehicle model. To determine the precise effect of the numerical algorithm on solutions, the numerical functions are listed and then the dynamic problem is also solved using the Hamming method, Runge-Kutta method, Newmark method, and finite difference method (FDM) using the MATLAB program. The relative precision of the methods is then discussed. In addition to the aforementioned descriptions, considering that low-amplitude vibration has a great effect on ride comfort, the vibration transmitted from the road is considered in this study. Thus, two criteria are selected for this study for the optimization and evaluation of the design of ride comfort, and then orthogonal experiments are used to determine the

effect of the parameters on the dynamic characteristics and the interaction effect. Then, two aims, such as the dynamic load coefficient and vertical acceleration, are selected as multi-objective optimization aims to analyze and optimize the vehicle's dynamic behavior. The optimized dynamic characteristic is then compared with the original result.

2 Vehicle model and road dynamics

In this section, the road-vehicle coupling dynamics model and performance indices, such as ride comfort, energy, and road handling, are discussed.

2.1 Condensation of the degrees of freedom

The model of vehicle dynamics can be established using traditional methods, modal synthesis, or nonlinear modeling methods. The traditional model was established using Newton's laws, the Lagrange equation, and D'Alembert's principle to derive differential equations. A quarter-vehicle model is shown in Fig. 1. The dynamic equations for the dynamic simulation model can be expressed as follows:

$$\begin{cases} m_1\ddot{z}_1' = K_t(q-z_1') - K_s(z_1'-z_2') + C_s(\dot{z}_1'-\dot{z}_2'), \\ m_2\ddot{z}_2' = K_s(z_1'-z_2') + C_s(\dot{z}_1'-\dot{z}_2'), \end{cases} \quad (1)$$

where m_2 represents the sprung mass, m_1 represents the unsprung mass, K_s and C_s are the stiffness and damping of the suspension, respectively, K_t is the tire stiffness, z_2' and z_1' are the displacements of the sprung and unsprung masses, respectively, and q is the road displacement input.
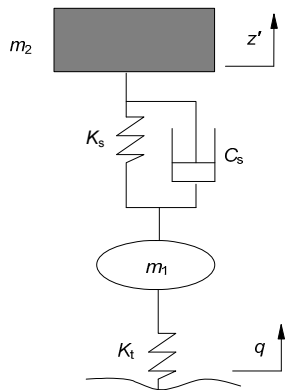

Fig. 1 A quarter-vehicle model

2.2 Half-vehicle model

When a vehicle runs on the road, the excitation of the rear and front tires is different owing to the excitation delay. The half-vehicle model with four DOFs is shown in Fig. 2. In this paper, the structure of the vehicle body is presented with respect to the central axis perpendicular to the vehicle's plane of symmetry, where M_{wf} is the unsprung mass on the front tire, M_{wr} is the unsprung mass on the rear tire, and M_{bh} is the mass of the body.

According to Fig. 2, the dynamic equations of the half-vehicle motion model can be written as follows:

$$\begin{cases} \ddot{z}_2 = \left(\dfrac{1}{M_{bh}} + \dfrac{ab}{J_b}\right)[K_{sf}(z_1-z_2) + C_{sf}(\dot{z}_1-\dot{z}_2)] \\ \qquad + \left(\dfrac{1}{M_{bh}} - \dfrac{b^2}{J_b}\right)[K_{sr}(z_3-z_4) + C_{sr}(\dot{z}_3-\dot{z}_4)], \\ \ddot{z}_3 = \dfrac{1}{M_{wr}}[K_{tr}(q_{tt}-z_3) - K_{sr}(z_3-z_4) - C_{sr}(\dot{z}_3-\dot{z}_4)], \\ \ddot{z}_4 = \left(\dfrac{1}{M_{bh}} - \dfrac{a^2}{J_b}\right)[K_{sf}(z_1-z_2) - C_{sf}(\dot{z}_1-\dot{z}_2)] \\ \qquad + \left(\dfrac{1}{M_{bh}} + \dfrac{ab}{J_b}\right)[K_{sr}(z_3-z_4) + C_{sr}(\dot{z}_3-\dot{z}_4)], \end{cases}$$

$$(2)$$

where z_1 and z_2 are the vertical displacements of the unsprung and sprung masses at the front axis, z_3 and z_4 are the vertical displacements of the unsprung and sprung masses at the rear axis and rear tires, and q_t and q_{tt} are the input displacements at the front and rear tires, respectively. φ is the roll angle of the body, a is the distance from the front axis to the center of mass, b is the distance from the rear axis to the center of mass, J_b is the moment of inertia of the body around the lateral axis, K_{tf} is the vertical stiffness of the front tire, K_{tr} is the vertical stiffness of the rear tire, K_{sf} is the stiffness of the front suspension, K_{sr} is the stiffness of the rear suspension, C_{sf} is the damping of the front suspension, and C_{sr} is the damping of the rear suspension.

2.3 Full-vehicle model

In this study, a seven-DOF vehicle model is established to analyze the dynamic motion of a vehicle.

This model consists of a sprung mass free to bounce, pitch, and roll, connected to four unsprung masses free to bounce vertically with respect to the sprung mass. The sprung mass has three DOFs representing the body bounce, pitch, and roll movement. The unsprung masses of the vehicle model have four DOFs, due to the vertical motions. Fig. 3 shows a seven-DOF full-vehicle model.

Much work based on the multi-DOF model has been conducted. However, the fundamental questions are still not clear. A detailed seven-DOF model can be established and its function written as follows:

$$
\begin{cases}
m_b \ddot{z}_b - C_{sA}(\dot{z}_{wA} - \dot{z}_{bA}) - K_{sA}(z_{wA} - z_{bA}) \\
\quad - C_{sB}(\dot{z}_{wB} - \dot{z}_{bB}) - K_{sB}(z_{wB} - z_{bB}) \\
\quad - C_{sC}(\dot{z}_{wC} - \dot{z}_{bC}) - K_{sC}(z_{wC} - z_{bC}) \\
\quad - C_{sD}(\dot{z}_{wD} - \dot{z}_{bD}) - K_{sD}(z_{wD} - z_{bD}) = 0, \\
I_p \ddot{\theta} + [C_{sA}(\dot{z}_{wA} - \dot{z}_{bA}) + K_{sA}(z_{wA} - z_{bA}) \\
\quad + C_{sB}(\dot{z}_{wB} - \dot{z}_{bB}) + K_{sB}(z_{wB} - z_{bB})]a \\
\quad - [C_{sC}(\dot{z}_{wC} - \dot{z}_{bC}) + K_{sC}(z_{wC} - z_{bC}) \\
\quad + C_{sD}(\dot{z}_{wD} - \dot{z}_{bD}) + K_{sD}(z_{wD} - z_{bD})]b = 0, \\
I_r \ddot{\varphi} - [C_{sA}(\dot{z}_{wA} - \dot{z}_{bA}) + K_{sA}(z_{wA} - z_{bA}) \\
\quad - C_{sB}(\dot{z}_{wB} - \dot{z}_{bB}) - K_{sB}(z_{wB} - z_{bB})]B_f \\
\quad - [C_{sC}(\dot{z}_{wC} - \dot{z}_{bC}) + K_{sC}(z_{wC} - z_{bC}) \\
\quad - C_{sD}(\dot{z}_{wD} - \dot{z}_{bD}) - K_{sD}(z_{wD} - z_{bD})]B_r = 0, \\
m_{wA} \ddot{z}_{wA} - K_{tA}(z_{gA} - z_{wA}) - C_{sA}(\dot{z}_{wA} - \dot{z}_{bA}) \\
\quad - K_{sA}(z_{wA} - z_{bA}) = 0, \\
m_{wB} \ddot{z}_{wB} - K_{tB}(z_{gB} - z_{wB}) - C_{sB}(\dot{z}_{wB} - \dot{z}_{bB}) \\
\quad - K_{sB}(z_{wB} - z_{bB}) = 0, \\
m_{wC} \ddot{z}_{wC} - K_{tC}(z_{gC} - z_{wC}) - C_{sC}(\dot{z}_{wC} - \dot{z}_{bC}) \\
\quad - K_{sC}(z_{wC} - z_{bC}) = 0,
\end{cases}
\tag{3}
$$

where I_p is the pitching moment of inertia, I_r is the roll moment of inertia, θ_b is the pitch angle of the body, φ is the roll angle of the body, m_{wA} is the unsprung mass at the left front tire, m_{wB} is the unsprung mass at the right front tire, m_{wC} is the unsprung mass at the left rear tire, m_{wD} is the unsprung mass at the right rear tire, K_{sA} is the stiffness of the suspension at the left front tire, K_{sB} is the stiffness of the suspension at the right front tire, K_{sC} is the stiffness of the suspension at the left rear tire, K_{sD} is the stiffness of the suspension at the right rear tire, C_{sA} is the damping of the sus-

pension at the left front tire, C_{sB} is the damping of the suspension at the right front tire, C_{sC} is the damping of the suspension at the left rear tire, C_{sD} is the damping of the suspension at the right rear tire, K_{tA} is the stiffness of the left front tire, K_{tB} is the stiffness of the right front tire, K_{tC} is the stiffness of the left rear tire, K_{tD} is the stiffness of the right rear tire, L is the distance between the shafts, B_f represents the distance between the front wheel and mass center, B_r represents the distance between the rear wheel and mass center, z_b is the vertical displacement of the center of mass, z_{bA} is the vertical displacement of the body endpoint at the left front tire, z_{bB} is the vertical displacement of the body endpoint at the right front tire, z_{bC} is the vertical displacement of the body endpoint at the left rear tire, z_{bD} is the vertical displacement of the body endpoint at the right rear tire, z_{gA} is the vertical displacement of the left front tire, z_{gB} is the vertical displacement of the right front tire, z_{gC} is the vertical displacement of the left rear tire, z_{gD} is the vertical displacement of the right rear tire, and m_b is the sprung mass of the body.
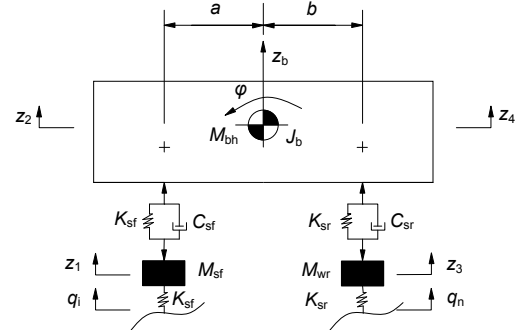

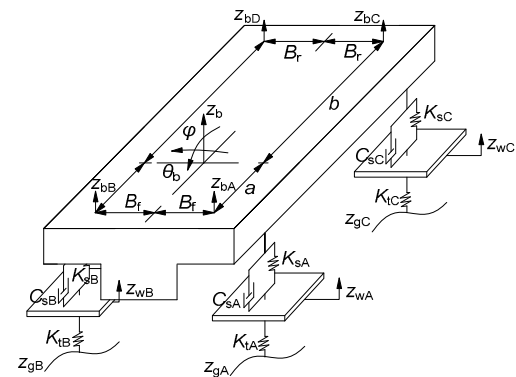**Fig. 2 A four-DOF half-vehicle model**

Fig. 3 A seven-DOF full-vehicle model

3 Road roughness model

Road excitation varies randomly over a wide range. A rough road can be typically represented by a stationary Gaussian stochastic process of a given displacement power spectral density (PSD) in $m^2/(m^{-1})$. To simulate the vehicle suspension system with road excitation, a road profile is defined as the cross-sectional shape of the road surface under the given conditions, which can be written as statistical procedures (Taghirad and Esmailzadeh, 1998; Zuo and Nayfeh, 2003). The relationships between the spatial frequency n and PSD function $G_q(n)$ can be approximated by two straight lines on a log-log scale, and expressed as

$$G_q(n) = G_q(n_0)\left(\frac{n}{n_0}\right)^{-W}, \quad n > 0, \qquad (4)$$

where n_0 is the reference spatial frequency, and the value of W is 2.0.

Mesh the region (n_1, n_2) into m sections using the PSD at the central frequency n_{mid_i} to represent the PSD over the entire region. The PSD at the ith section can be expressed as follows:

$$q_1 = S_q(n_{mid\_i})\Delta n_i, \qquad i = 1, 2, \cdots, m, \qquad (5)$$

where $\Delta n_i = (n_2 - n_1)/(m+1)$ is the interval frequency in this section.

For every small section, the standard deviation for every frequency n_{mid_i} is $\sqrt{2G_q(n_{mid\_i})\Delta n_i}$ and its sine wave function can be expressed as

$$q' = \sqrt{2G_q(n_{mid\_i})\Delta n_i}\ \sin(2\pi n_{mid\_i}x + \theta_i). \qquad (6)$$

Overlaying the sine wave function in each section simultaneously, the frequency domain of the random pavement displacement can be expressed as

$$q(x) = \sum_{i=1}^{n}\sqrt{2G_q(n_{mid\_i})\Delta n_i}\ \sin(2\pi n_{mid\_i}x + \theta_i), \qquad (7)$$

where x is the displacement along longitudinal direction, and θ is the random value in the region of $(0, 2\pi)$.

The signal in Eq. (7) is in frequency domain, which needed to be transformed to the time domain.

The frequency domain pavement random with the time input form can be expressed as

$$q(t) = \sum_{i=1}^{n}\sqrt{2G_q(f_{mid\_i})\Delta f_i'}\sin(2\pi f'_{mid\_i}t + \theta_i), \qquad (8)$$

where $f' = u \cdot n$, the center frequency in the ith region $f'_{mid\_i} = u \cdot n_{mid\_i}$, $x/u = t$, and u is the vehicle velocity.

The dynamics of the vehicle are always sensitive to road roughness. Road roughness is very important in vehicle design, so it has been studied for a long time. It can be described by wheel track elevation profiles. Recently, the effects of the road profile on the ride comfort of a vehicle have been widely studied. Road profiles must be described in a statistical way because of their random profile. The International Standardization Organization (ISO) proposed a method that classifies road roughness using power spectral density functions. Table 1 shows the power spectral density of road roughness log scale plots proposed by the ISO, which are in eight classes (from A to H). They are approximated using two straight lines. Class H indicates the roughest road profile, whereas class A indicates the smoothest road profile. Through numerous measurements, the ISO suggested a road classification scheme based on the degree of road roughness S_0 (Zuo and Zhang, 2013) (Table 1).

For the simulation of a vehicle undergoing random road excitation, road roughness expressed in the time domain with class B is shown in Fig. 4. This is also the load excitation in the analysis below. Additionally, excitation can also be expressed in the frequency domain, and it needs to be transformed into the distance domain using an inverse Fourier transform. Fig. 5 presents three classes of road profiles (classes B, C, and D), which are expressed in the distance domain.

Table 1 Parameters for different classes of road

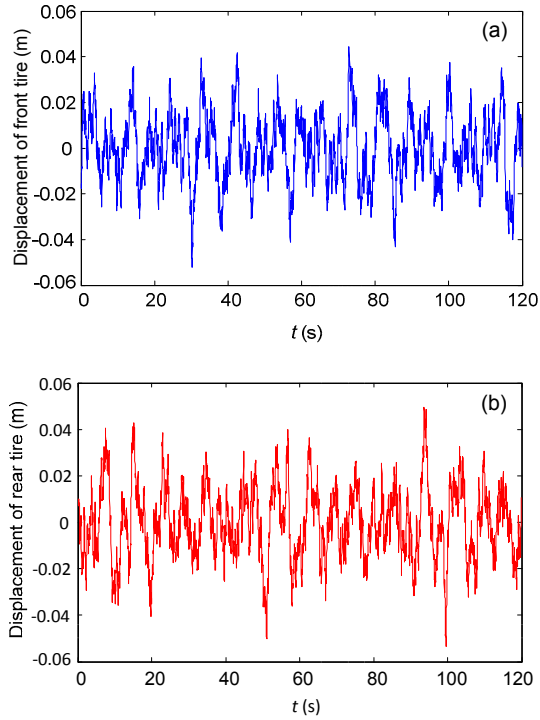| Road class	S_0 range ($\times 10^{-6}$ m^2/(cycle/m))	S_0 mean ($\times 10^{-6}$ m^2/(cycle/m))
A (very good)	<8	4
B (good)	8–32	16
C (average)	32–128	64
D (poor)	128–512	256
E (very poor)	512–2048	1024
F	2048–8192	4096
G	8192–32 768	16 384
H	>32 768	

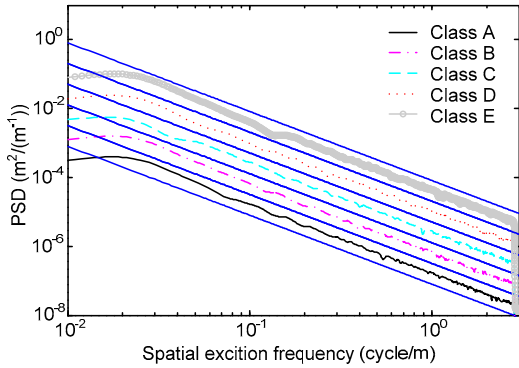**Fig. 4 Road excitation of the front (a) and rear (b) tires**

Fig. 5 Excitation PSD of the vehicle

4 Method for solving the dynamic simulation

There are many methods for solving the dynamic simulation of a vehicle. In this study, different types of numerical methods are introduced to solve the multi-DOF vehicle model. The typical numerical methods for solving linear dynamic equations are the Newmark method, FDM, finite element method, Wilson method, and Runge-Kutta method.

The dynamic equation for the mass matrix can be expressed as

$$M \frac{d^2 z}{dt^2} + C \frac{dz}{dt} + Kz = f, \tag{9}$$

where $z=(z_1, z_2, ..., z_n)$, M is the mass matrix composed of different vehicle parts, C is the damping matrix composed of different vehicle parts, K is the stiffness matrix composed of different vehicle parts, and f is the excitation force.

4.1 Finite difference method

There are two ways for second-order linear ordinary differential equations to be discretized into finite difference equation. One is to use the difference instead of the derivative; the other is to use the integral interpolation method. The highest order derivative in equation is reduced to one order, so the requirement for z smoothness is weakened. Assume that the calculation regarding the dynamics is in the region of $[a', b']$, then the integration of Eq. (9) over the interval $[x', x'']$ can be written as

$$\left[M \frac{dz}{dt} \right]_{x''} - \left[M \frac{dz}{dt} \right]_{x'} + \int_{x'}^{x''} C \frac{dz}{dt} dt + \int_{x'}^{x''} Kz dt = \int_{x'}^{x''} f dt. \tag{10}$$

Meshing the region $[a', b']$ into N parts, every node can be expressed as $t=a'+ih$ ($0 \leq i \leq N$, and h is the step), and the finite difference equation in the mesh region with respect to time $t_{i-1/2}$ and $t_{i+1/2}$ about x' and x'' can be written as

$$\left[M \frac{dz}{dt} \right]_{t_{i+1/2}} - \left[M \frac{dz}{dt} \right]_{t_{i-1/2}} + \int_{t_{i-1/2}}^{t_{i+1/2}} C \frac{dz}{dt} dt + \int_{t_{i-1/2}}^{t_{i+1/2}} Kz dt = \int_{t_{i-1/2}}^{t_{i+1/2}} f dt. \tag{11}$$

The integral terms in Eq. (11) can be represented by rectangular formulas, and they can be written as

$$\int_{t_{i-1/2}}^{t_{i+1/2}} C \frac{dz}{dt} dt = hC \frac{dz_i}{dt} + O(h^3),$$

$$\int_{t_{i-1/2}}^{t_{i+1/2}} Kz dt = hKz_i + O(h^3), \tag{12}$$

$$\int_{t_{i-1/2}}^{t_{i+1/2}} f dt = hf_i + O(h^3).$$

Submitting Eq. (12) into Eq. (11) and neglecting the error part $O(h^3)$, and using z_i to represent $[z]_i$,

Eq. (11) can be rewritten as

$$M\frac{z_{i+1}-2z_i+z_{i-1}}{h}+C\frac{z_{i+1}-z_{i-1}}{2}+hKz_i=hf_i. \quad (13)$$

4.2 Revised Hamming method

For initial value of the differential problems:

$$\begin{cases} \dot{y}=f(x,y), & a<x\le b, \\ y(a)=y_0. \end{cases} \quad (14)$$

When the numerical solution is carried out, because $y_0, y_1, \ldots, y_n$ have been obtained, the calculation formula can be constructed using this information. It can also reduce the amount of calculation, and obtain the higher accuracy. The general expression can be written as

$$y_{n+1}=\sum_{k=0}^{r}\alpha_k y_{n-k}+h\sum_{k=-1}^{r}\beta_k f_{n-k}. \quad (15)$$

Eq. (15) can be expanded based on Taylor's theorem, so the fourth-order and four-step explicit function can be written as

$$y_{n+1}=y_{n-3}+\frac{4h}{3}(2f_n-f_{n-1}+2f_{n-2}). \quad (16)$$

The local truncation error for Eq. (13) can be written as

$$\varepsilon_{n+1}=\frac{14}{45}h^5 y^{(5)}(\xi)+O(h^6). \quad (17)$$

Another Hamming method with a fourth-order and three-step explicit function can be written as

$$y_{n+1}=\frac{1}{8}(9y_n-y_{n-2})+\frac{3h}{8}(f_{n+1}+2f_n-f_{n-1}), \quad (18)$$

where the local truncation error for Eq. (18) is

$$\varepsilon_{n+1}=-\frac{1}{40}h^5 y^{(5)}(\xi)+O(h^6).$$

Eq. (16) and Eq. (18) are combined to obtain the prediction-correction formula:

$$\begin{cases} y_{n+1}^p=y_{n-3}+\frac{4h}{3}(2f_n-f_{n-1}+2f_{n-2}), \\ y_{n+1}=\frac{1}{8}(9y_n-y_{n-2})+\frac{3h}{8}[f(x_{n+1},y_{n+1}^p)+2f_n-f_{n-1}]. \end{cases} \quad (19)$$

5 Design of experiments

The design of experiments (DOE) is important as a formal way to maximize information gained while minimizing required resources, especially for the orthogonal experiment. It can identify the main effects of every input variable on global aim responses when optimizing vehicle dynamic behavior. In this paper, six input variables with three levels are used, as shown in Table 2. Some outputs are selected to evaluate lubrication performance, such as dynamic acceleration and the dynamic load coefficient (He *et al.*, 2015).

Six input parameters with three levels for each parameter imply a set of 3^6 runs for the entire experiment with one change at a time. Every experiment to perform the simulation requires at least 5 h. Thus, 5×3^7 min is required to achieve the goal. To overcome this problem, the orthogonal experiment, which consists of one component with three levels, is introduced. The DOE $L(3^7)$ is described as a 64 design of resolution. This means that an overall number of $n=6$ factors is studied, which only requires at least 320 min. However, the variables' interaction is neglected in the experiment. In future work, an experiment considering the variables' interaction will also be designed.

6 Multi-objective optimization theory

There are several objective functions in the literature for optimizing the ride comfort of a vehicle. A single-objective optimizer is always used to solve the ride comfort problem to obtain one optimum solution. However, it is always difficult to obtain the desired result using this optimization technique, so the multi-objective approach is used to optimize the ride comfort of the vehicle. There are two multi-objective optimization approaches to optimize the ride comfort of a vehicle: the weighted-sum approach and Pareto-based approaches. The weighted-sum approach is a classical multi-objective optimization approach in

Table 2 Orthogonal experiment

Influence factor No.	Variable	Variable meaning	Value		
			Level 1	Level 2	Level 3
A	K_{sA} (N/m)	Stiffness of front suspension	15 300	17 000	18 700
B	K_{sC} (N/m)	Stiffness of rear suspension	19 800	22 000	24 200
C	C_{sA} (N·s/m)	Damping of front suspension	1350	1500	1650
D	C_{sC} (N·s/m)	Damping of rear suspension	1350	1500	1650
E	K_t (N/m)	Stiffness of tire	172 800	192 000	211 200
F	a (m)	Distance from mass center to front axis	1.125	1.25	1.375
G	b (m)	Distance from mass center to rear axis	1.359	1.51	1.661

which all the objectives are weighted and added together to form a single objective. However, it is always difficult to define the weighted coefficient using this method. In this paper, root mean square (RMS) acceleration with human vibration-sensitivity and the response force to tire are selected as the aims to optimize. Thus, a multi-objective optimization problem with a number of minimized or maximized functions can be solved. By applying the non-dominated sorting genetic algorithm (NSGA)-II to the above problem, a set of optimal solutions (a Pareto front) is obtained for the suspension system design. In the following, the multi-objective optimization problem (MOOP) is stated in its general form of

$$\begin{cases} f(\boldsymbol{x}) = \min[f_1(\boldsymbol{x}), f_2(\boldsymbol{x}), \cdots, f_m(\boldsymbol{x})], \\ \text{subject to} \ \ g_i(\boldsymbol{x}) = 0, \ j = 1, 2, \cdots, i, \\ \qquad h_k(\boldsymbol{x}) \geq 0 \ \text{or} \ \leq 0, \ k = 1, 2, \cdots, k, \\ \qquad x_{il} \leq x_i \leq x_{iu}, \ i = 1, 2, \cdots, n, \end{cases} \quad (20)$$

where $\boldsymbol{x} = [x_1, x_2, \ldots, x_n]$, and $g_i(\boldsymbol{x})$ and $h_k(\boldsymbol{x})$ are the equality and inequality constraint functions, respectively.

NSGA was first proposed by Srinivas and Deb (1994). However, there are many defects in this optimization, such as: (1) the number of non-domination sorting algorithm calculations is too high, in particular, when the size of the population increases, the number of calculations increases rapidly; (2) no elitist preservation method; (3) need to set sharing parameters σ. Later, the researchers changed the algorithm, and it is developed NSGA-II. The algorithm uses the crowding and crowding comparison operators to retain the best individual among the parents to go into the next generation to ensure the algorithm obtains the best solution. Non-dominated sorting is performed for

every generation of the parent and offspring. The detailed process of NSGA-II is explained as follows:

1. In this study, the decision variables are the width of bearing, radius of the journal, and viscosity of the oil film. The method uses a random number generator to produce n populations of individuals, where each individual within the population represents a possible solution, and population initialization is the basis for subsequent operations.

2. Individual numerical information in the group is read into a MATLAB program, and its fitness values are calculated through their objective function.

3. When fast non-dominated sorting is performed, there is a n_i and a p_i corresponding at each individual set after different individuals compared with each other. n_i and p_i are generated by the individual of the non-dominated sequence rank i. Thus, fast non-dominated sorting is completed. The calculation of the individual crowding corresponds to each non-dominated set.

4. Given crossover probability P_c, all individuals will be paired off. Let P_1 and P_2 be the parent individuals, C_1 and C_2 the child self, and V the string length. Quantity V of random number R_i is produced in the region [0, 1] before crossing, where $1 \leq i \leq V$. Parent individuals that satisfy $R_i < P_c$ perform the gene exchange, and new individuals are produced.

5. The offspring and parents mix together after genetic manipulation. Repeat steps 2 and 3 and then select half the population according to non-dominated sorting. This can take the best individual parent into the next generation. The population level can be rapidly promoted.

As mentioned previously, two criteria were selected for this study for optimization and evaluation of the design of ride comfort. Additionally, some parameters from the suspension system were considered as design variables, including the suspension

spring stiffness and hydraulic damper coefficient of four tires. The indices for the problem are then defined as

$$F_1 = \sqrt{\frac{1}{N}\sum_{t=1}^{N}\left|\ddot{z}_b\right|^2}, \tag{21}$$

$$F_2 = \sqrt{\frac{1}{N}\sum_{t=1}^{N}\left|\frac{\dfrac{F_{d1}(t)}{G_1} + \dfrac{F_{d2}(t)}{G_2} + \dfrac{F_{d3}(t)}{G_3} + \dfrac{F_{d4}(t)}{G_4}}{4}\right|^2}, \tag{22}$$

where F_{di} and G_i are respectively the dynamic load and static load that the tire acts on the ground ($G_1 = m_b g \dfrac{b}{a+b} \cdot \dfrac{b_l'}{b_l'+b_r'}$, $G_2 = m_b g \dfrac{b}{a+b} \cdot \dfrac{b_r'}{b_l'+b_r'}$,

$G_3 = m_b g \dfrac{a}{a+b} \cdot \dfrac{b_r}{b_l+b_r}$, $G_4 = m_b g \dfrac{a}{a+b} \cdot \dfrac{b_l}{b_l+b_r}$, b_l' is the distance between the body endpoint at the left front tire and the mass center, b_r' is the distance between the body endpoint at the right front tire and the mass center, b_l is the body endpoint at the left rear tire and the mass center, b_r is the body endpoint at the right rear tire and the mass center). In this study, $b_l'=b_r'=B_f$, $b_l=b_r=B_r$. F_1 is the vertical acceleration root mean square of the vehicle, and F_2 is the dynamic load coefficient of the tire.

The excitation forces of the four tires are composed of Eq. (22) and they can be written as

$$\begin{cases} F_{d1} = C_{sA}(\dot{z}_{wA} - \dot{z}_b + a\dot{\theta} - B_f\dot{\varphi}) \\ \qquad + K_{sA}(z_{wA} - z_b + a\theta - B_f\varphi) + m_{wA}\ddot{z}_{wA}, \\ F_{d2} = C_{sB}(\dot{z}_{wB} - \dot{z}_b + a\dot{\theta} + B_f\dot{\varphi}) \\ \qquad + K_{sB}(z_{wB} - z_b + a\theta - B_f\varphi) + m_{wB}\ddot{z}_{wB}, \\ F_{d3} = C_{sC}(\dot{z}_{wC} - \dot{z}_b - b\dot{\theta} + B_r\dot{\varphi}) \\ \qquad + K_{sC}(z_{wC} - z_b - b\theta + B_r\varphi) + m_{wC}\ddot{z}_{wC}, \\ F_{d4} = C_{sD}(\dot{z}_{wD} - \dot{z}_b - b\dot{\theta} - B_r\dot{\varphi}) \\ \qquad + K_{sC}(z_{wD} - z_b - b\theta - B_r\varphi) + m_{wD}\ddot{z}_{wD}. \end{cases} \tag{23}$$

The optimization satisfies the following constraints:

$$\begin{aligned} f_{d1} &= z_b - a\theta + B_f\varphi - z_{bA}, \\ f_{d2} &= z_b - l_f\theta - B_f\varphi - z_{bB}, \\ f_{d3} &= z_b + b\theta - B_r\varphi - z_{bC}, \end{aligned} \tag{24}$$

$$\begin{aligned} f_{d4} &= z_b + b\theta + B_r\varphi - z_{bD}, \\ 0 &\le f_{di} \le [f_d], \quad i = 1, 2, 3, 4, \end{aligned}$$

where f_{di} is the travel for every suspension, and $[f_d]$ is the maximum travel for the suspension.

7 Parameters and numerical process

Input data for the quarter-vehicle model, half-vehicle model, and full-vehicle model are provided in Tables 3–5. The type of vehicle is a Ford Granada, which has been widely researched. The relevant parameters are selected from the relevant research and Yu and Lin (2005). In this study, the analysis is mainly focused on the numerical solution method and optimization method. Some parameters are limited to a range to determine the optimum result; thus, the basic parameters are known. These parameters near their regions can be changed, and the multi-objective optimization method is performed to search the parameters set in their regions. First, different types of vehicle models are established and different types of

Table 3 Relevant quarter-vehicle parameter values

Vehicle parameter	Value
Sprung mass, m_2 (kg)	317.5
Unsprung mass, m_1 (kg)	45.4
Suspension stiffness, K_s (N/m)	22 000
Tire stiffness, K_t (N/m)	192 000
Suspension damping, C_s (N·s/m)	1520

Table 4 Relevant half-vehicle parameter values

Vehicle parameter	Value
Sprung mass, M_{bh} (kg)	690
Moment of inertia, J_b (kg·m²)	1222
Front axle unsprung mass, M_{wf} (kg)	40.5
Rear axle unsprung mass, M_{wr} (kg)	45.4
Distance from center of gravity to front axle for wheel, a (m)	1.25
Distance from center of gravity to rear axle for wheel, b (m)	1.51
Front suspension stiffness, K_{sf} (N/m)	17 000
Rear suspension stiffness, K_{sr} (N/m)	22 000
Front suspension damping, C_{sf} (N·s/m)	1500
Rear suspension damping, C_{sr} (N·s/m)	1500
Front tire stiffness, K_{tf} (N/m)	192 000
Rear tire stiffness, K_{tr} (N/m)	192 000

Table 5 Relevant full-vehicle parameter values

Vehicle parameter	Value
Vehicle mass, m_b (kg)	1380
Pitch moment of inertia, θ_b (kg·m^2)	2444
Roll moment of inertia, φ (kg·m^2)	380
Front axle left unsprung mass, m_{wA} (kg)	40.5
Front axle right unsprung mass, m_{wB} (kg)	40.5
Rear axle left unsprung mass, m_{wC} (kg)	45.4
Rear axle right unsprung mass, m_{wD} (kg)	45.4
Front left suspension stiffness, K_{sA} (N/m)	17 000
Front right suspension stiffness, K_{sB} (N/m)	17 000
Rear left suspension stiffness, K_{sf} (N/m)	22 000
Rear right suspension stiffness, K_{sr} (N/m)	22 000
Front left suspension damping, C_{sA} (N·s/m)	1500
Front right suspension damping, C_{sB} (N·s/m)	1500
Rear left suspension damping, C_{sC} (N·s/m)	1500
Rear right suspension damping, C_{sD} (N·s/m)	1500
Front left tire stiffness, K_{tA} (N/m)	192 000
Front right tire stiffness, K_{tB} (N/m)	192 000
Rear left tire stiffness, K_{tC} (N/m)	192 000
Rear right tire stiffness, K_{tD} (N/m)	192 000
Distance from center of gravity to front axle for wheel, a (m)	1.25
Distance from center of gravity to rear axle for wheel, b (m)	1.51
Front wheel-base, B_f (m)	0.74
Rear wheel-base, B_r (m)	0.74

algorithms are applied to these models. The precision of the calculations are compared, and the reason for the precision difference is explained. In addition to the aforementioned analyses, the seven-DOF vehicle model (full-vehicle model) is selected as the basic model to design the experiment. The effects of the parameters on vibration and tire excitation are listed, and then an approximate model is established. Surface response analysis is also performed, and then the NSGA-II algorithm is used to solve the above problem. Because the aim of this study is to improve the vibration performance of the vehicle based on the multi-objective theory, the variable of all the input parameters satisfies $a'{\leq}x{\leq}b'$. In this paper, from the constraint of all the variables, it can be concluded that: $15\,300{\leq}K_{sA}{\leq}18\,700$, $19\,800{\leq}K_{sC}{\leq}24\,200$, $1350{\leq}C_{sA}{\leq}1650$, $1350{\leq}C_{sC}{\leq}1650$, $172\,800{\leq}K_t{\leq}211\,200$, and $2.484{<}a{+}b{<}3.036$. All the analysis is based on the seven-DOF model. In future work, a new model with more DOFs will be built, and then a more precise prediction model can be obtained. It is expected that

the difference arises from the negligibility of some details and the rough algorithm in the present theory.

8 Results and discussion

8.1 Characteristics comparison under a different model

In this study, two traditional methods, the Runge-Kutta method and Newmark method, are selected to compare with the FDM and Hamming method. Fig. 6 shows the vertical acceleration of the vehicle based on a two-DOF vehicle system; some results in this region have been expanded because they were too dense. The results show that the acceleration values calculated by these four methods agree well with each other.

Fig. 7 shows the vertical acceleration and pitch acceleration values calculated by the four-DOF vehicle model. Different types of solving methods are compared. To gain an insight into the results, they are expanded in some time regions. The results show that the acceleration values calculated by these four methods also agree well with each other.

Fig. 8 shows the seven-DOF model for the entire vehicle. It compares different types of solving methods to gain an insight into the results. The results are expanded in some time regions and show that the acceleration values calculated by these four methods also agree well with each other. However, the waving trend in the same time-expanded region is not the same.

According to the above analysis, it is difficult to determine the precise difference calculated by different models. In fact, in realistic engineering, the
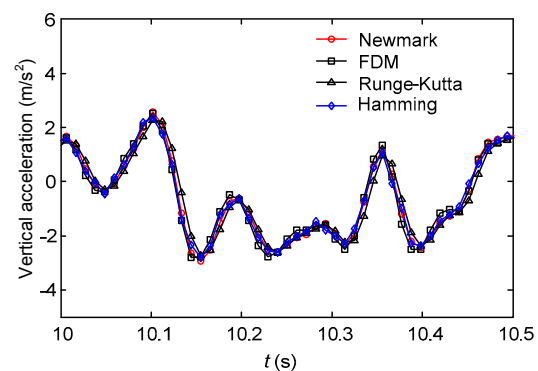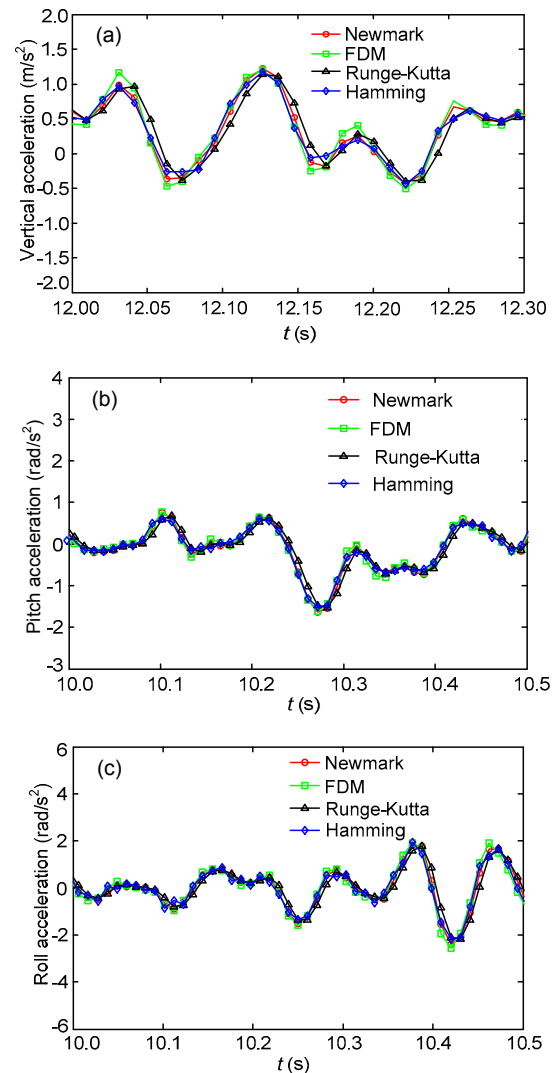

Fig. 6 Comparison of vertical acceleration among different methods in two DOFs
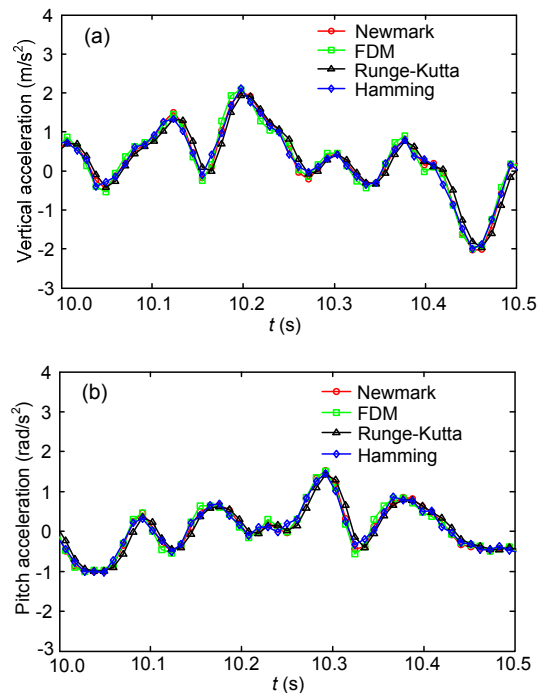
Fig. 7 Comparison of vertical acceleration and pitch acceleration among different methods in four DOFs: (a) vertical acceleration; (b) pitch acceleration

RMS of the acceleration is usually used to evaluate the vibration performance of the vehicle. Thus, the RMS of the acceleration calculated by different models and different algorithms are listed in Table 6. The results show that there is little difference for the RMS of the vertical acceleration among these results calculated by different models based on two DOFs. The results calculated by the Runge-Kutta and Hamming methods are 1.2428 m/s^2 and 1.2500 m/s^2, respectively, which are less than the Newmark method and FDM. Compared with the two-DOF model, the result calculated by the four-DOF model is smaller, and the errors of the vertical acceleration for these four methods can achieve 53.74%, 52.28%, 53.11%, and 52.83%, respectively. The vertical acceleration calculated by the Runge-Kutta or Hamming method based on the two-DOF model is close to that for the four-DOF model. These two methods are better than the Newmark method and FDM; their errors are less than approximately 3.9%–4.7% in terms of the vertical acceleration and 4.6%–5.5% in terms of the pitch acceleration. Comparing the errors for the four-DOF model among these four methods, the results show that the Runge-Kutta and Hamming methods are also close to the seven-DOF model.

Fig. 8 Comparison of vehicle acceleration with different methods in seven DOFs for the entire vehicle: (a) vertical acceleration; (b) pitch acceleration; (c) roll acceleration

Compared with the four-DOF model, the result calculated by the seven-DOF model is smaller, and the errors of the vertical acceleration for the four methods can achieve 5.11%, 5.54%, 4.84%, and 4.90%, respectively. The errors of the Newmark method and FDM are larger than approximately 3.7%–4.1% in terms of the vertical acceleration and 5.9%–9% in terms of the pitch acceleration.

A detailed analysis is performed to analyze why the Runge-Kutta and Hamming methods are better. The results calculated by the FDM and Newmark method are less precise because these two methods need to call four steps. This will lead the error to average; thus, it causes the error of the entire result to

increase. However, the FDM and Newmark method only need to call for the former step result; thus, they accumulate the error. The Runge-Kutta method obtains the result of the broken line, which is relatively smooth, in a large deviation node position. It requires approximately three steps to approach a good result. The correction value is a slower speed solution. The Hamming law also requires three steps to adjust the numerical results, and they oscillate up and down around the true values of the approach point.

Table 7 also presents the calculation time for different numerical methods, and the results show that when the model changes from the quarter-vehicle model to full-vehicle model, the calculation time increases. The calculation time for the revised Hamming method is longer than that for the other three methods. The calculation time for the Runge-Kutta method increases significantly for the full-vehicle model.

Fig. 9 shows the comparison of the dynamic characteristics based on different models. Because the quarter-vehicle model only considers vertical acceleration and the half-vehicle model only considers vertical acceleration and pitch acceleration, only the PSDs of vertical acceleration and pitch acceleration are shown. The results show that the error of the quarter-vehicle model is larger compared with the other two models, but their trends are the same, and the half-vehicle model is nearly the same as the full-vehicle model. In the comparison of pitch acceleration, there is some difference between the half-vehicle model and full-vehicle model, but this error is very small and it only appears at the peak position. Thus, the analysis that follows will be performed using the seven-DOF model to evaluate the dynamic characteristics of the vehicle.
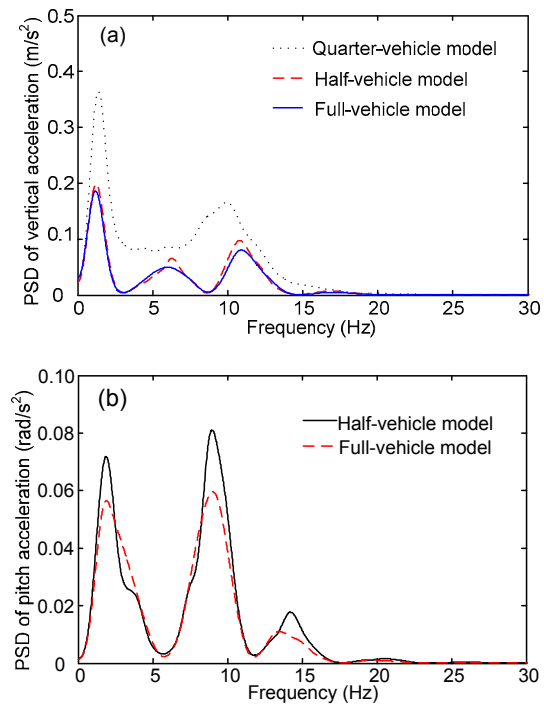
Fig. 9 Comparison of the dynamic characteristics based on different models: (a) vertical acceleration; (b) pitch acceleration

Table 6 Comparison of acceleration RMS values in different DOFs

Parameter		RMS (m/s²)			
		Newmark	FDM	Runge-Kutta	Hamming
2-DOF	Dynamic deflection	0.0101	0.0102	0.0101	0.0106
	Vertical acceleration	1.3082	1.3074	1.2428	1.2500
4-DOF	Vertical acceleration	0.8509	0.8585	0.8117	0.8179
	Pitch acceleration	0.6196	0.6141	0.5832	0.5855
7-DOF	Vertical acceleration	0.8095	0.8134	0.7742	0.7797
	Pitch acceleration	0.5949	0.5872	0.5616	0.5641
	Roll acceleration	0.6436	0.6806	0.5942	0.6056

Table 7 Comparison of calculation time for different numerical methods

Model	Calculation time (s)			
	Newmark	FDM	Runge-Kutta	Hamming
Quarter-vehicle model	0.0554	0.0298	0.0070	0.2524
Half-vehicle model	0.0573	0.0600	0.0153	0.2850
Full-vehicle model	0.0746	0.0806	0.2216	0.3414

8.2 Effect of parameters on the evolution index

To determine the effect of some parameters on the dynamic characteristics of the vehicle, the effect of pavement grade and vehicle speed on the dynamic load of the tire and the vertical acceleration of the vehicle mass center are calculated based on the seven-DOF model. Fig. 10a shows the effect of vehicle speed on the dynamic load of the tire under different pavement grades. The results show that the dynamic load coefficient increases with the speed, the amplitude for grades A and B is very small, and the dynamic load increases clearly with speed, especially for pavement grade D. The same result can be seen in Fig. 10b.
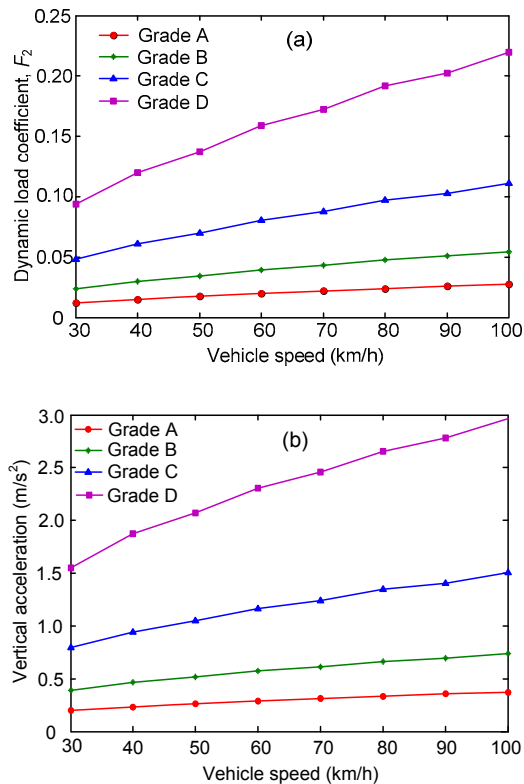

Fig. 10 Effect of vehicle speed on the dynamic load (a) and vertical acceleration (b) under different pavement grades

Fig. 11 shows the effect of pavement grade on the vertical acceleration and dynamic load for different vehicle speeds. The results show that vertical acceleration and dynamic load coefficient increase with speed. When the pavement grade changes from A to D, the road becomes rough; hence, these two characteristics increase.
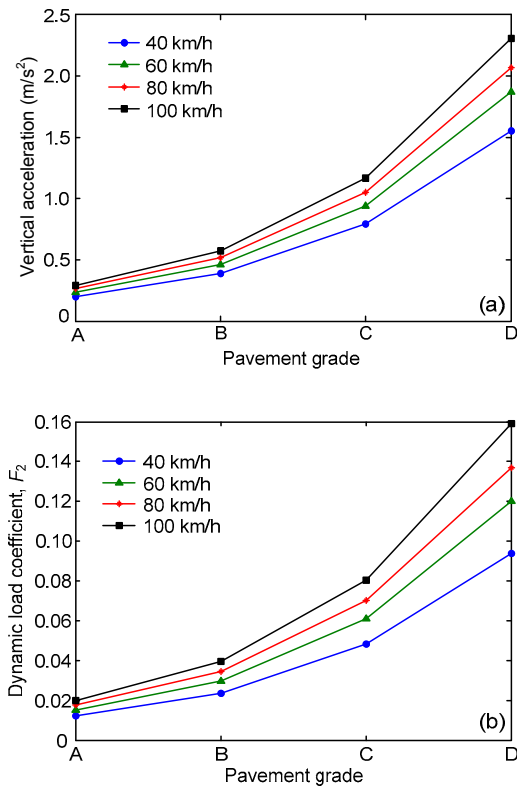

Fig. 11 Effect of pavement grade on the vertical acceleration (a) and dynamic load coefficient (b) for different vehicle speeds

8.3 Effect of parameters on the evolution index

There are many factors that affect the dynamic characteristics of a vehicle, such as suspension stiffness, suspension damping, unsprung mass, vehicle mass, and tire stiffness. These parameters are always coupled together to affect the evolution indices, and how one parameter affects the evolution indices is always easy to understand. In this section, the rule for the parameters on the characteristics must be known. If the vehicle design manifests some problems, the reason can be obtained quickly by investigating the effect of the parameters. To determine how suspension stiffness and damping affect the dynamic characteristics, Fig. 12 shows the effect of suspension stiffness and damping on the PSD of the dynamic characteristics. Fig. 12a shows the PSD of the dynamic characteristics with different

suspensions: K=17 000 N·m and K=10 000 N·m. The results show that the PSD of the dynamic load coefficient is greatly different in the range 0–5 Hz. The amplitude decreases when the stiffness decreases in this region. There is little difference from the range 5–15 Hz (greater difference appears at the region of 10 Hz) and the amplitude is the same in the region of 15–30 Hz. Thus, there is no effect of improving the PSD of the dynamic characteristics by changing the suspension stiffness. Compared with suspension stiffness, damping nearly has an effect on all the frequency regions (0–30 Hz), as shown in Fig. 12b. When damping increases from 900 to 1500 N·s/m, the dynamic load coefficient decreases quickly in the vicinity of 1.226 Hz and 10.5 Hz; the value difference can achieve 0.00047 and 0.00088, respectively. Additionally, the order of magnitude for the damping effect is obviously higher than that for stiffness.

Figs. 12c and 12d show the effect of suspension stiffness and damping on the PSD of vertical acceleration. The results also show that the stiffness also only affects the frequency in the range 0–5 Hz; there

is nearly no effect in the range 5–30 Hz. Compared with stiffness, damping has an effect on vertical acceleration in the entire frequency region (0–30 Hz). However, the results clearly show that the contribution of stiffness and damping to the PSD of vertical acceleration are nearly the same, which is unlike their effect on the dynamic load coefficient. From the above analysis, the results show that the PSD of the dynamic characteristics can be improved by changing the suspension stiffness and damping according to different frequency problems.

8.4 DOE analysis for the dynamic characteristics

The factors dominating the dynamic load coefficient and vertical acceleration can be identified through their levels. The parameters that weight the effect of dynamic load coefficient (R_{DLC}) and vertical acceleration (R_{VC}) on every performance can be written as follows:

$$R_{DLC} = \max(R_i) - \min(R_i), \quad (25)$$

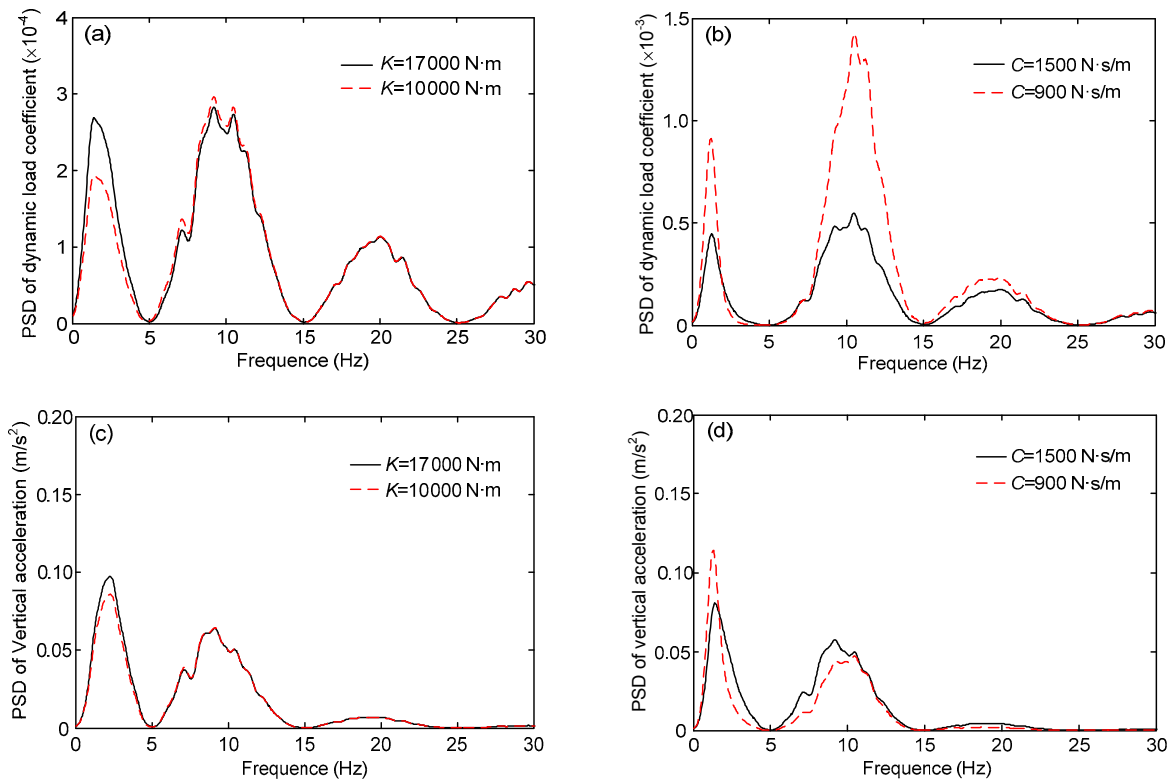$$R_{VC} = \max(R_i) - \min(R_i). \quad (26)$$

Fig. 12 Effect of stiffness *K* and damping *C* on the dynamic load and vertical acceleration: (a) effect of stiffness on the dynamic load coefficient; (b) effect of damping on the dynamic load coefficient; (c) effect of stiffness on vertical acceleration; (d) effect of damping on vertical acceleration

According to Eqs. (25) and (26), the effect of the input parameters on the dynamic load coefficient (F_2) and vertical acceleration (F_1) responses is analyzed, as shown in Fig. 13. The effect of the aforementioned seven factors on the dynamic load coefficient can be arranged as B>A>E>D>C>F>G; the dominating weight of the aforementioned seven factors on vertical acceleration can be arranged as E>G>F>D>C>A>B. In fact, there are some other indexes in the dynamic analysis of the vehicle. If the best vehicle that has the smallest vibration is desired, the multi-objective function needs to be established and the weight power of every aim also needs to be set, and then a suitable design can be obtained.
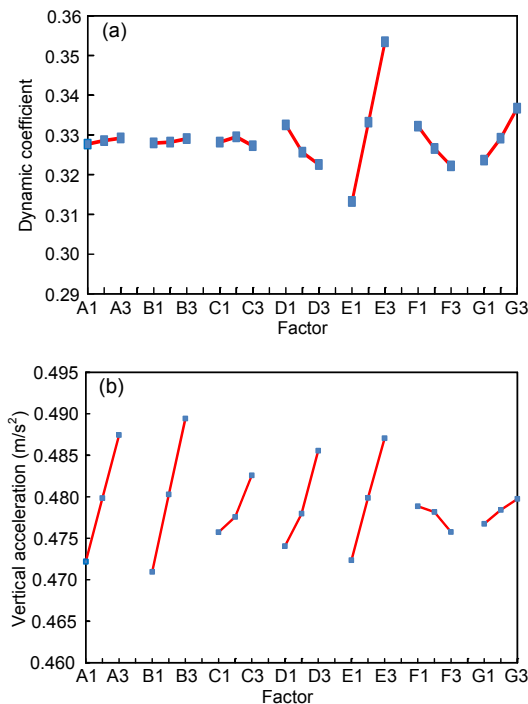
Fig. 13 Weight comparison of factors: (a) comparison of the dynamic load coefficient by various factors and their levels; (b) comparison of the vertical acceleration by various factors and their levels

In fact, the parameters' interaction is always neglected. In this paper, the Pareto effect of all the parameters and parameters' interaction are all investigated. The results show clearly that the contribution of all the parameters can be arranged as B>E>A>D>C>G>F, as shown in Fig. 14a. There is little difference from the above orthogonal experiment. The reason for this difference will be researched in future

work. In addition to the above, the parameters' interactions C_{sA}-K_{sA}, a-K_{sA}, and C_{sA}-K_t also have an effect on F_1, to some extent, so the parameters' interaction cannot be neglected. The results also show that the contribution of some parameters are negative, such as C_{sA}-K_{sA}, a-K_{sA}, and a. Fig. 14b shows the contribution of the parameters and parameters' interaction to F_2. The results show that the contribution of all the parameters can be arranged as E>G>F>D>B. This result agrees well with the orthogonal experiment. In addition to the above discussion, some parameters' interactions also make a contribution to F_2, such as a-b, C_{sC}-K_t, a-K_t, and b-K_t. Thus, when analysis regarding the effect of the parameters on the aim is performed, the parameters cannot be neglected; it may contribute more than a single parameter to the aim.
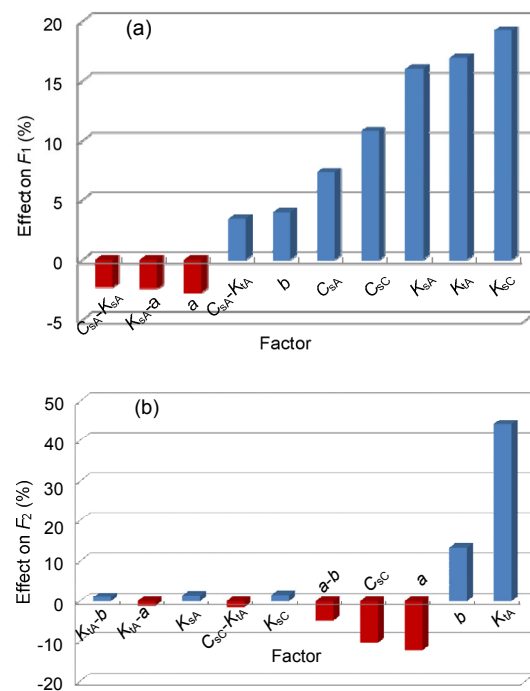
Fig. 14 Pareto effect of all the parameters: (a) contribution of all the parameters and parameters' interaction to F_1; (b) contribution of all the parameters and parameters' interaction to F_2

8.5 Optimization analysis

This section describes the details of the GA, which is fitted to solve the vehicle dynamic optimization problem. Seven design variables, the stiffness

of the front suspension (K_{sA}), stiffness of the rear suspension (K_{sC}), damping of the front suspension (C_{sA}), damping of the rear suspension (C_{sC}), stiffness of the tire (K_t), distance from the mass center to front axis (a), and distance from the mass center to rear axis (b), are selected to control the vehicle's dynamic performance. The mass of the vehicle, moment of pitch inertia of the vehicle, moment of roll inertia of the vehicle, distance between the tires, and mass of the upspring are fixed for two reasons: (1) the mass is always related to the moment of inertia; there is a complex relationship between these variables and the variation of mass around this point is substantially small; (2) the distance between the tires is always fixed. Therefore, these design variables are omitted. Thus, a rank-based GA with niche operator and 'separate pool scheme' is used to optimize the two objective functions, the minimum dynamic load coefficient and the minimum vertical acceleration, under many constraints. The binary coded NSGA-II using three digits for each variable is chosen. The total population is 100 members and the population size is 40, with a crossover probability of 0.9 and crossover distribution of index 10, and a mutation distribution of index 20 is considered. A constraint on the total distance between the front axis and rear axis (2.484 m<$a+b$<3.036 m), i.e., f_{d1}, f_{d2}, f_{d3}, and f_{d4}< 30 mm, is imposed.

Fig. 15 illustrates the results obtained for vehicle dynamics. The Pareto frontier can be clearly seen (round point) from the results of the dynamic load coefficient and vertical acceleration for the Pareto design variables. There are many optimized results in the multi-objective optimization analysis. These results form a set and they move to a small region after the calculation and form an edge, as shown in Fig. 15. One of these results is the optimal result. The reason for using the Pareto approach in this study is to show that when the multi-objective optimization is performed, the optimal results are not always the only results; they form a set. Simultaneously, the entire optimization process is reflected in this figure, for example, the initial parameters used to calculate the aim are located at position *B*, and then the next calculation aim will achieve position *C* which is closer to the optimal result. However, this value is not the optimal result. After some calculations, the result becomes closer to the Pareto edge.

Table 8 presents the comparison of parameters and results before and after optimization. The results show that the solution F_1 reduces by 0.0352 m/s², which is an improvement of 7.22%, and the solution F_2 reduces by 0.0225, which is an improvement of 6.82% after optimization. The parameters changed, to some extent. The close agreement between the expected and predicted data shows that NSGA-II can be used to obtain optimized results in the theoretical program.

To verify the results, Fig. 16 also shows the comparison of the PSD of the vertical acceleration and dynamic load coefficient before and after optimization. The results show that nearly all the information is optimized over the entire frequency region.

9 Conclusions

Based on the dynamic simulation of different vehicle systems, a study to establish the two-DOF,
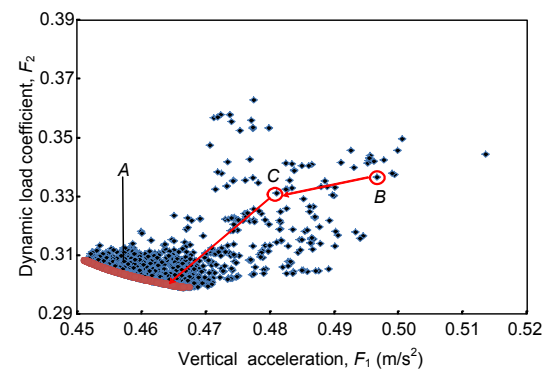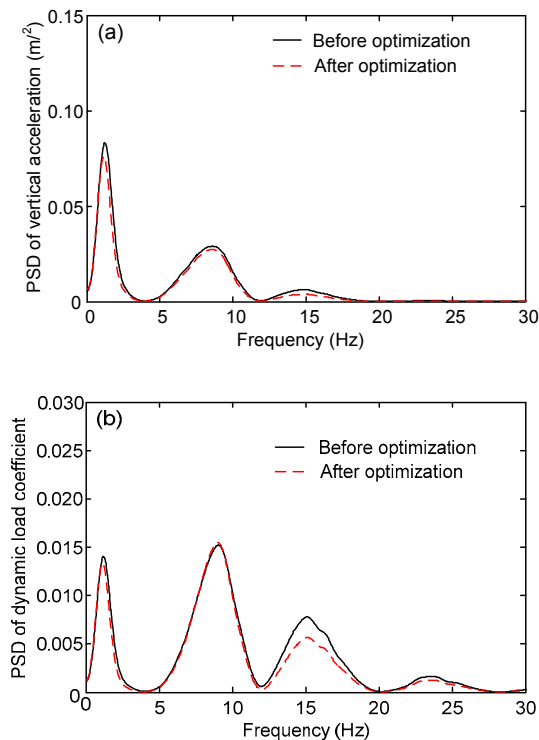

Fig. 15 All the Pareto designs after 4000 generations

Table 8 Parameters and results comparison

Status	a (m)	b (m)	K_{sA} (N/m)	K_{sC} (N/m)	C_{sA} (N·s/m)	C_{sC} (N·s/m)	K_t (N/m)	F_1 (m/s²)	F_2
Before optimization	1.25	1.51	17 000	20 000	1500	1500	192 000	0.4871	0.3300
After optimization	1.37	1.36	15 301	19 800	1353	1366	172 800	0.4519	0.3075

Fig. 16 Comparison of the PSD of vertical acceleration (a) and dynamic load coefficient (b) after optimization

four-DOF, and seven-DOF models was performed in a simulation program. Different types of numerical methods used to solve the dynamic simulation equation were studied. Multi-objective optimization was introduced to optimize the vibration of the vehicle. The effects of the parameters on the dynamic characteristics were all investigated, and the precision of the average acceleration was compared. The conclusions are summarized as follows:

1. In the multi-degree system, the results calculated by these four methods agreed well with each other. The Hamming method was a new method that could calculate the dynamic characteristic of the system, and it was better than the Newmark method and FDM. The average acceleration was also used for comparison. The Runge-Kutta method was better than the four-step Hamming method. The Hamming method calls former steps. An error exists at every step, which leads to the RMS being larger than that for the Runge-Kutta method, but this does not affect precision.

2. Orthogonal experiments were combined to identify the factors dominating the vehicle's dynamic

behavior. The effect of the weight of the aforementioned seven factors on the dynamic load coefficient can be arranged as E>G>F>D>C>A>B. The dominating weight of the aforementioned seven factors on vertical acceleration can be arranged as B>A>E>D>C>F>G. Thus, this technique can be used to find the effect of the parameters on the ride comfort of the vehicle.

3. Orthogonal experiments can be used to determine the parameters of the dynamic characteristics. In fact, some parameters always couple with each other to affect characteristics; the interaction effect sometimes has a greater effect on the vehicle's dynamic behavior, and these effects are always neglected.

4. The overall objective raised in this study integrates the problem of the complex dynamic modeling of a vehicle and an optimization process characterized by a high number of variables to be simultaneously modified and a high number of constraints to be satisfied. After the optimization analysis, the results showed that the optimal results were not always the only results; there are many optimized results in the multi-objective optimization analysis and these results form a set. They move to a small region after the calculation and form an edge, which is called a Pareto edge. One optimum result shows that the solution F_1 reduces by 0.0352 m/s^2, which is an improvement of 7.22%, and the solution F_2 reduces by 0.0225, which is an improvement of 6.82% after optimization. In a practical design, it is better to couple the DOE with the multi-objective optimization method to perform the optimization, which can avoid trapping in a local minimum or maximum, because the sample can distribute the entire space after the design of the experiment.

References

Bae, D.S., Lee, J.K., Cho, H.J., *et al.*, 2000. An explicit integration method for realtime simulation of multibody vehicle models. *Computer Methods in Applied Mechanics and Engineering*, **187**(1-2):337-350.
　　http://dx.doi.org/10.1016/S0045-7825(99)00138-3

Baumal, A., McPhee, J., Calamai, P., 1998. Application of genetic algorithms to the design optimization of an active vehicle suspension system. *Computer Methods in Applied Mechanics and Engineering*, **163**(1-4):87-94.
　　http://dx.doi.org/10.1016/S0045-7825(98)00004-8

Campbell, C., 1981. Automotive Suspensions. Chapman Hall, London, UK.

Ekoru, J.E.D., Pedro, J.O., 2013. Proportional-integral-derivative control of nonlinear half-car electro-hydraulic suspension systems. *Journal of Zhejiang University-SCIENCE A (Applied Physics & Engineering)*, **14**(6): 401-416.
http://dx.doi.org/10.1631/jzus.A1200161

Gündoğdu, O., 2007. Optimal seat and suspension design for a quarter car with driver model using genetic algorithms. *International Journal of Industrial Ergonomics*, **37**(4): 327-332.
http://dx.doi.org/10.1016/j.ergon.2006.11.005

Gupta, T.C., 2007. Identification and experimental validation of damping ratios of different human body segments through anthropometric vibratory model in standing posture. *Journal of Biomechanical Engineering*, **129**(4): 566-574.
http://dx.doi.org/10.1115/1.2720917

He, Z., Sun, Y., Zhang, G., 2015. Tribiological performances of connecting rod and by using orthogonal experiment, regression method and response surface methodology. *Applied Soft Computing*, **29**:436-449.
http://dx.doi.org/10.1016/j.asoc.2015.01.009

Hegazy, S., Rahnejat, H., Hussain, K., 1999. Multi-body dynamics in full-vehicle handling analysis. *Proceedings of the Institution of Mechanical Engineers, Part K: Journal of Multi-body Dynamics*, **213**(1):19-31.
http://dx.doi.org/10.1243/1464419991544027

Ikenaga, S., Lewis, F.L., Campos, J., *et al.*, 2000. Active suspension control of ground vehicle based on a full-vehicle model. American Control Conference, **6**:4019-4024.

Jamali, A., Shams, H., Fasihozaman, M., 2014. Pareto multi-objective optimum design of vehicle-suspension system under random road excitations. *Proceedings of the Institution of Mechanical Engineers, Part K: Journal of Multi-body Dynamics*, **228**(3):282-293.
http://dx.doi.org/10.1177/1464419314531757

Kadir, Z.A., Hudha, K., Ahmad, F., *et al.*, 2012. Verification of 14DOF full vehicle model based on steering wheel input. *Applied Mechanics and Materials*, **165**:109-113.
http://dx.doi.org/10.4028/www.scientific.net/amm.165.109

Mirzaei, M., Hassannejad, R., 2007. Application of genetic algorithms to optimum design of elasto-damping elements of a half-car model under random road excitations. *Proceedings of the Institution of Mechanical Engineers, Part K: Journal of Multi-body Dynamics*, **221**(4):515-526.
http://dx.doi.org/10.1243/14644193JMBD101

Nasir, M.Z.M., Hudha, K., Amir, M.Z., *et al.*, 2012. Modelling, simulation and validation of 9 DOF vehicles model for automatic steering system. *Applied Mechanics and Materials*, **165**:192-196.
http://dx.doi.org/10.4028/www.scientific.net/amm.165.192

Nigam, S.P., Malik, M., 1987. A study on a vibratory model of a human body. *Journal of Biomechanical Engineering*, **109**(2):148-153.
http://dx.doi.org/10.1115/1.3138657

Rao, S.S., 1996. Engineering Optimization. John Wiley & Sons, New York, USA.

Reddy, P.S., Ramakrishna, A., Ramji, K., 2015. Study of the dynamic behaviour of a human driver coupled with a vehicle. *Proceedings of the Institution of Mechanical Engineers, Part D: Journal of Automobile Engineering*, **229**(2):226-234.
http://dx.doi.org/10.1177/0954407014537642

Schmitke, C., Morency, K., McPhee, J., 2008. Using graph theory and symbolic computing to generate efficient models for multi-body vehicle dynamics. *Proceedings of the Institution of Mechanical Engineers, Part K: Journal of Multi-body Dynamics*, **222**(4):339-352.
http://dx.doi.org/10.1243/14644193JMBD160

Soleymani, M., Montazeri-Gh, M., Amiryan, R., 2012. Adaptive fuzzy controller for vehicle active suspension system based on traffic conditions. *Scientia Iranica*, **19**(3):443-453.
http://dx.doi.org/10.1016/j.scient.2012.03.002

Srinivas, N., Deb, K., 1994. Multiobjective function optimization using nondominated sorting genetic algorithms. *Evolutionary Computation*, **2**(3):221-248.
http://dx.doi.org/10.1162/evco.1994.2.3.221

Sulaiman, S., Samin, P.M., Jamaluddin, H., *et al.*, 2012. Modeling and validation of 7-DOF ride model for heavy vehicle. International Conference on Automotive, Mechanical and Materials Engineering, p.108-112.

Taghirad, H., Esmailzadeh, E., 1998. Automobile passenger comfort assured through LQG/LQR active suspension. *Journal of Vibration and Control*, **4**(5):603-618.
http://dx.doi.org/10.1177/107754639800400504

Tamboli, J.A., Joshi, S.G., 1999. Optimum design of passive suspension system of a vehicle subjected to actual random road excitations. *Journal of Sound and Vibration*, **219**(2): 193-205.
http://dx.doi.org/10.1006/jsvi.1998.1882

Thite, A.N., Banvidi, S., Ibicek, T., *et al.*, 2011. Suspension parameter estimation in the frequency domain using a matrix inversion approach. *Vehicle System Dynamics*, **49**(12):1803-1822.
http://dx.doi.org/10.1080/00423114.2010.544319

Vaddi, P.K.R., Kumar, C.S., 2014. A non-linear vehicle dynamics model for accurate representation of suspension kinematics. *Proceedings of the Institution of Mechanical Engineers, Part C: Journal of Mechanical Engineering Science*, **229**(6):1002-1014.
http://dx.doi.org/10.1177/0954406214542840

von Chappuis, H., Mavros, G., King, P.D., *et al.*, 2013. Prediction of impulsive vehicle tyre-suspension response to abusive drive-over-kerb manoeuvres. *Proceedings of the Institution of Mechanical Engineers, Part K: Journal of Multi-body Dynamics*, **227**(2):133-149.
http://dx.doi.org/10.1177/1464419312469756

Yu, F., Lin, Y., 2005. Vehicle System Dynamics. Machinery Industry Press, Beijing, China (in Chinese).

Yuen, T.J., Foong, S.M., Ramli, R., 2014. Optimized suspension

kinematic profiles for handling performance using 10-degree-of-freedom vehicle model. *Proceedings of the Institution of Mechanical Engineers, Part K: Journal of Multi-body Dynamics*, **228**(1):82-99.
http://dx.doi.org/10.1177/1464419313516436

Zong, C., Song, P., Hu, D., 2011. Estimation of vehicle states and tire-road friction using parallel extended Kalman filtering. *Journal of Zhejiang University-SCIENCE A (Applied Physics & Engineering)*, **12**(6):446-452.
http://dx.doi.org/10.1631/jzus.A1100056

Zuo, L., Nayfeh, S.A., 2003. Structured H2 optimization of vehicle suspensions based on multi-wheel models. *Vehicle System Dynamics*, **40**(5):351-371.
http://dx.doi.org/10.1076/vesd.40.5.351.17914

Zuo, L., Zhang, P.S., 2013. Energy harvesting, ride comfort, and road handling of regenerative vehicle suspensions. *Journal of Vibration and Acoustics*, **135**(1):011002.
http://dx.doi.org/10.1115/1.4007562

中文概要

题　目：基于数值算法的车辆动力学模型及数值求解方法精度的对比研究

目　的：通过采用不同数值方法求解不同的车辆动力学模型，为车辆动力学模型研究提供参考；结合正交试验和多目标优化算法来分析各个参数对车辆性能的影响权重，采用多目标优化算法进行车辆动力学多目标优化分析，为车辆的设计提供参考依据。

创新点：研究不同数值方法的求解精度，为车辆动力学求解方法提供新途径；采用正交试验设计研究车辆各参数的影响权重，为车辆设计提供参考；采用多目标优化算法设计车辆，能兼顾车辆多个方面的性能。

方　法：采用不同动力学求解算法、正交试验设计和多目标优化分析方法。

结　论：1. 基于不同数值求解算法的研究表明，Hamming法要优于 Newmark 法和有限差分法，四阶Hamming法的精度不如龙格库塔法；2. 正交试验可得到各参数对车辆动力学的影响权重，但忽略了参数间的交互效应；3. 经过多目标优化设计，衡量车辆振动性能的两个指标分别减少了 7.22% 和 6.82%。

关键词：车辆；Hamming 法；龙格库塔法；数值算法；动力仿真